

1 **Structural basis for potent inhibition of D-amino acid**  
2 **oxidase by thiophene carboxylic acids**

3

4 Yusuke Kato<sup>a</sup>, Niyada Hin<sup>b</sup>, Nobuo Maita<sup>a</sup>, Ajit G. Thomas<sup>b</sup>, Sumire Kurosawa<sup>a</sup>,  
5 Camilo Rojas<sup>b</sup>, Kazuko Yorita<sup>a</sup>, Barbara S. Slusher<sup>b,c</sup>, Kiyoshi Fukui<sup>a,\*</sup> and  
6 Takashi Tsukamoto<sup>b,c</sup>

7

8 <sup>a</sup>Institute for Enzyme Research, Tokushima University, Tokushima 770-8503,  
9 Japan.

10 <sup>b</sup>Johns Hopkins Drug Discovery and <sup>c</sup>Department of Neurology, Johns Hopkins  
11 University, Baltimore, MD 21205, USA

12

13 \*Corresponding author. Tel.: +81-88-633-7429; e-mail:  
14 [kiyo.fukui@tokushima-u.ac.jp](mailto:kiyo.fukui@tokushima-u.ac.jp)

15

16 **Abstract**

17 A series of thiophene-2-carboxylic acids and thiophene-3-carboxylic acids  
18 were identified as a new class of DAO inhibitors. Structure-activity relationship  
19 (SAR) studies revealed that small substituents are well-tolerated on the  
20 thiophene ring of both the 2-carboxylic acid and 3-carboxylic acid scaffolds.  
21 Crystal structures of human DAO in complex with potent thiophene carboxylic  
22 acids revealed that Tyr224 was tightly stacked with the thiophene ring of the  
23 inhibitors, resulting in the disappearance of the secondary pocket observed with  
24 other DAO inhibitors. Molecular dynamics simulations of the complex revealed  
25 that Tyr224 preferred the stacked conformation irrespective of whether Tyr224  
26 was stacked or not in the initial state of the simulations. MM/GBSA indicated a  
27 substantial hydrophobic interaction between Tyr244 and the thiophene-based  
28 inhibitor. In addition, the active site was tightly closed with an extensive network  
29 of hydrogen bonds including those from Tyr224 in the stacked conformation. The  
30 introduction of a large branched side chain to the thiophene ring markedly  
31 decreased potency. These results are in marked contrast to other DAO inhibitors  
32 that can gain potency with a branched side chain extending to the secondary  
33 pocket due to Tyr224 repositioning. These insights should be of particular

1 importance in future efforts to optimize DAO inhibitors with novel scaffolds.

2

### 3 **Keywords**

4 Flavoenzyme; schizophrenia; drug discovery; X-ray crystallography; molecular  
5 dynamics

6

### 7 **Highlights**

- 8 · Therapeutics with DAO/DAAO inhibition is a potential approach to treat  
9 schizophrenia.
- 10 · Thiophene carboxylic acids were identified as a new class of DAO inhibitors.
- 11 · Tyr224 of DAO was tightly stacked with the thiophene ring of the inhibitors.
- 12 · The hydrophobic interaction and hydrogen bonds between them induced the  
13 stacking.
- 14 · The results should be important in future efforts to optimize DAO inhibitors.

15

### 16 **Abbreviations**

17 DAO/DAAO, D-amino acid oxidase; D-Ser, D-serine; SAR, Structure-activity  
18 relationship; MD, molecular dynamics; H-bond, hydrogen bond; DOPA,  
19 dihydroxyphenylalanine; CPC, 4-(4-chlorophenethyl)-1H-pyrrole-2-carboxylic  
20 acid; TPC, 4*H*-thieno[3,2-*b*]pyrrole-5-carboxylic acid; MM/GBSA, molecular  
21 mechanics energies combined with the generalized Born and surface area

22

23

## 24 **1. Introduction**

25 D-Amino acid oxidase (DAO/DAAO) is a flavoenzyme that catalyzes the  
26 oxidation of D-amino acids, producing the corresponding  $\alpha$ -keto acids, ammonia,  
27 and hydrogen peroxide [1]. One of the endogenous substrates for DAO in the  
28 brain is the co-agonist of NMDA receptors, D-serine (D-Ser) [2-4]. In the brains  
29 of patients with schizophrenia, the amount of D-Ser decreases presumably due  
30 to increased DAO activity [5-10]. Since NMDA receptor hypofunction is believed  
31 to play a pathophysiological role in the negative symptoms and cognitive  
32 impairment of schizophrenia, inhibition of DAO has been of great interest as a  
33 therapeutic approach distinct from those targeting dopaminergic pathways

1 [11-13]. Indeed, the past decade has seen a wave of medicinal chemistry efforts  
2 in the search for new DAO inhibitors [14, 15].

3 Nearly all DAO inhibitors possess a carboxylic acid or its bioisostere which  
4 interacts with Tyr228 and Arg283 residues that are responsible for recognizing  
5 the carboxylate group of D-amino acid substrates. The majority of DAO inhibitors  
6 also contain an aromatic ring despite DAO's ability to oxidize a wide range of  
7 neutral D-amino acids including those with an aliphatic chain [16, 17]. This is at  
8 least partially due to the ability of the aromatic ring to form a  $\pi$ - $\pi$  interaction with  
9 FAD's isoalloxazine ring [18]. According to the structural studies, the aromatic  
10 ring of benzoate and its derivative are stacked with the side chain of Tyr224  
11 [18-20]. However, other inhibitors and products including  
12 4*H*-thieno[3,2-*b*]pyrrole-5-carboxylic acid (TPC),  
13 4-(4-chlorophenethyl)-1*H*-pyrrole-2-carboxylic acid (CPC) and imino DOPA are  
14 not stacked with Tyr224 because the side chain of Tyr224 moves away from the  
15 active site [21, 22]. The stacked and displaced states of Tyr224 are referred to  
16 as S and D states, respectively, in this paper. The conformational flexibility of  
17 Tyr224 plays a critical role in the structural plasticity of the substrate-binding site  
18 of DAO, which catalyzes a wide range of D-amino acid substrates. In the D state,  
19 an additional pocket (referred to as the secondary pocket) is created as a result  
20 of the movement of Tyr224 to accommodate DAO inhibitors/products with a  
21 branched side chain (see **Fig. 1B, D**). Although the precise mechanism by which  
22 the conformation of Tyr224 is regulated is poorly understood, the secondary  
23 pocket has been exploited in a number of new DAO inhibitors containing a  
24 branched chain [22-24].

25 In a search for new scaffolds that inhibit DAO, we screened a variety of  
26 aromatic carboxylic acids. Among them, thiophene-2-carboxylic acid **1a** and  
27 thiophene-3-carboxylic acid **2a (Table 1)** exhibited low micromolar inhibitory  
28 potency with IC<sub>50</sub> values of 7.8  $\mu$ M and 4.4  $\mu$ M, respectively. Herein we report  
29 structure-activity relationship (SAR) studies on the two thiophene-based  
30 scaffolds as well as X-ray crystallographic analysis and molecular dynamics  
31 simulations of the complex between thiophene-based compounds and DAO to  
32 elucidate the mechanism underlying their potent interactions.

## 2. Results

### 2.1. Inhibition of D-amino acid oxidase by low molecular weight thiophene carboxylic acids

Given that a number of D-amino acid oxidase (DAO/DAAO) inhibitors reported to date are aryl carboxylic acids, we screened a variety of molecules in this category in a search for new scaffolds that inhibit DAO. Our screening efforts identified thiophene-2-carboxylic acid **1a** and thiophene-3-carboxylic acid **2a** as low micromolar DAO inhibitors with IC<sub>50</sub> values of 7.8 μM and 4.4 μM, respectively. While compound **2a** was previously reported as a DAO inhibitor [25], compound **1a** represents a new scaffold for DAO inhibition. Although other aryl carboxylic acids were previously reported to exhibit substantially higher inhibitory potency, the low molecular weights of these compounds present attractive structural features as lead compounds and prompted us to evaluate their analogs in the DAO assay. In the first phase of SAR studies, we examined analogs with minimal changes in molecular size. All compounds but one (compound **1j**) were commercially available. As shown in **Scheme 1**, compound **1j** was obtained by fluorination of aldehyde **3** followed by hydrolysis of the methyl ester group.

The results are summarized in **Table 1**. Among compounds with the thiophene-2-carboxylic acid scaffold, many of the 5-substituted analogs, particularly those with a small substituent, potently inhibited DAO. For instance, 5-fluoro (**1b**), 5-chloro (**1c**) and 5-bromo (**1d**) analogs exhibited substantial improvement compared to the parent compound **1a**. While 5-methyl (**1e**) was found to be nearly as potent as **1a**, a gradual decrease in potency was seen with the increase in the size of the 5-substituents as shown by 5-difluoromethyl (**1f**) and 5-trifluoromethyl (**1g**) analogs. Inhibitory activity was completely abolished when a formyl group was incorporated into the 5-position (**1h**). Small substituents were also well tolerated in the 4-position as seen for **1i** and **1j**. Interestingly, 4,5-disubstituted analogs such as **1k** and **1l** represented the most potent DAO inhibitors within the thiophene-2-carboxylic acid series with IC<sub>50</sub> values of 0.09 and 0.36 μM, respectively. In contrast, any substitution at the 3-position appears to be detrimental to inhibitory activity as neither 3-fluoro (**1n**) nor 3-methyl (**1o**) analogs inhibited DAO. Incorporation of carboxylic acid

1 bioisosteres such as tetrazole (**1p** and **1q**) and boronic acid (**1r**) into the  
2 2-position also resulted in a complete loss of potency. As for the analogs of  
3 thiophene-3-carboxylic acid **2a**, 5-chloro (**2b**) and 5-methyl (**2c**) derivatives  
4 showed substantially improved potency as compared to the parent compound  
5 **2a**. Indeed, 5-chlorothiophene-3-carboxylic acid **2b** was the most potent  
6 thiophene-carboxylic acid-based DAO inhibitors with an IC<sub>50</sub> value of 0.04 μM.  
7 2,5-Dichloro analog **2d**, however, exhibited much weaker inhibitory potency.

8

## 9 **2.2. Preference for the S state in the complexes with 1c and 2b**

10 For a better understanding of the good potency of low molecular thiophene  
11 carboxylic acids, we determined the crystal structures of the **1c**-DAO and  
12 **2b**-DAO complexes (**Supplementary Table 1, Figs. 1, 2**). We found that the  
13 thiophene rings of the thiophene-2-carboxylic **1c** and thiophene-3-carboxylic **2b**  
14 acid analogs are stacked with the benzene ring of Tyr224. Thus, both of the  
15 complexes are in the S state in which the formation of the secondary pocket is  
16 lost due to the movement of Tyr224 (**Fig. 1**). The shapes and locations of **1c** and  
17 **2b** in the complexes are almost superimposable, with the exception of the sulfur  
18 atom of the thiophene ring (**Fig. 2**). Slight differences were observed for the  
19 shapes of the thiophene rings and the orientations of the carboxylate and  
20 chlorine atom. These may cause the difference in the IC<sub>50</sub> values between **1c**  
21 and **2b** (**Supplementary Fig. 1**).

22 To assess the stability of the S state conformation, we performed all-atom  
23 molecular dynamics (MD) simulations using the dimer crystal structure of the  
24 **2b**-DAO complex as an initial structure. We measured the distance between the  
25 centroids of the thiophene ring of **2b** and benzene ring of Tyr224 to judge  
26 whether Tyr224 was in the S or D state. The crystal structure of the **2b**-DAO  
27 complex shows a distance of ~4 Å between the two centroids. Based on visual  
28 inspection of the trajectories of the **2b**-DAO complex, we defined the S state as  
29 having a ~4 Å distance between the two centroids and the D state as having a  
30 distance that was ≥ ~5 Å .

31 The distance between the centroids of the thiophene ring of **2b** and benzene  
32 ring of Tyr224 of Chain A was ~4 Å most of the simulation time, while it  
33 occasionally became ≥ 5 Å (**Fig. 3A**). Thus the S state was dominant in the

1 equilibration between the S and D states. We measured the corresponding  
2 distance in Chain B as well in the same MD run; the results were reproducible  
3 (**Supplementary Fig. 2**). Repeated MD runs again gave similar results.

4 In contrast, the crystal structure of the TPC-DAO complex (PDB code: 3znn)  
5 shows the D state as seen in the imino DOPA-DAO complex [21, 22]. The  
6 secondary pocket in the TPC-DAO complex is unoccupied, because TPC is a  
7 planar molecule without a branched side chain (**Supplementary Table 2**). Thus,  
8 it would be possible to form the S state for the TPC-DAO complex without a  
9 steric clash between TPC and DAO's residues including Tyr224. However, MD  
10 using 3znn as an initial structure indicated that the distance between the  
11 centroids of the pyrrole ring of TPC and benzene ring of Tyr224 remained ~5 Å  
12 most of the time (i.e. the D state) (**Fig. 3B**). Repeated MD runs gave similar  
13 results reproducibly (**Supplementary Fig. 3**).

14 To exclude the possibility that the initial structures biased the results above,  
15 we performed additional MD runs with a virtual initial state in which **2b** was  
16 substituted for TPC in the D state TPC-DAO complex (**Fig. 3C, Supplementary**  
17 **Fig. 4**). The results showed that the S state became dominant within a few  
18 nanoseconds after the simulations were initiated. Conversely, MD runs with an  
19 initial state in which TPC was substituted for **2b** in an S state structure showed  
20 that the D state became dominant over time (**Fig. 3D, Supplementary Fig. 5**).  
21 These simulations suggest that the S state is thermodynamically preferred for  
22 the **2b**-DAO complex while DAO adopts the D state when **TPC** is bound to its  
23 active site.

### 24 25 **2.3. Thiophene carboxylic acids containing a branched chain as DAO** 26 **inhibitors**

27 In light of the previous findings that some DAO inhibitor scaffolds benefit from  
28 an added branched side chain that occupies the secondary pocket, we  
29 examined whether such a modification can also improve the inhibitory potency of  
30 the thiophene carboxylic acid scaffolds. The previously reported SAR studies  
31 indicate that the incorporation of a side chain to the position across from the  
32 carboxylate attached carbon is most effective in other aryl carboxylic acid-based  
33 DAO inhibitors. This prompted us to evaluate 4- or 5-substituted derivatives of

1 thiophene-2-carboxylic acid (compounds **1s-w**) as well as 5-substituted  
2 derivatives of thiophene-3-carboxylic acid (compounds **2e-f**). While some of  
3 these compounds were commercially available, compounds **1u**, **1w**, and **2f** were  
4 synthesized using bromothiophenes as starting materials. The key steps  
5 involved in the synthesis include Sonogashira coupling and subsequent catalytic  
6 hydrogenation as illustrated in **Schemes 2** and **3**.

7 As summarized in **Table 2**, none of these compounds showed substantial  
8 inhibitory activity against DAO. The lack of potency seen with these compounds  
9 represent a sharp contrast to other aryl carboxylic acid scaffolds that benefited  
10 from side chain incorporation. For example, a 4-substituted pyrrole-2-carboxylic  
11 acid discovered by Sunovion, SEP-137, inhibits DAO with a markedly higher  
12 potency [22] than the unsubstituted pyrrole-2-carboxylic acid [26]. Similar  
13 structural modifications to **1a** and **2a**, however, led to a complete or significant  
14 loss of potency as demonstrated by compounds **1u**, **1w**, and **2f**. It is worth noting  
15 that a much smaller substituent such as ethyl group is sufficient enough to  
16 eliminate the ability to inhibit DAO as seen with compounds **1s**, **1v**, and **2e** even  
17 though the corresponding methyl substituted derivatives **1e**, **1i**, and **2c** showed  
18 potent DAO inhibition (**Table 1**). These results suggest that DAO is incapable of  
19 accommodating thiophene carboxylic acids with a branched side chain larger  
20 than a methyl group. The S state observed in the co-crystal structures of DAO  
21 with **1c** and **2b** appears to have little flexibility in responding to the branched side  
22 chain added to the thiophene ring by shifting to the D state and creating the  
23 secondary binding pocket.

#### 24 25 **2.4. Mechanism to stabilize the S state**

26 We calculated the binding free energy ( $\Delta G_{\text{bind}}$ ) by molecular mechanics  
27 energies combined with the generalized Born and surface area (MM/GBSA)  
28 using MD trajectories to compare  $\Delta G_{\text{bind}}$  with  $\Delta G_{\text{exp}}$  that was derived from  
29 experimental  $\text{IC}_{50}$  (**Table 3**).  $\Delta G_{\text{bind}}$  and  $\Delta G_{\text{exp}}$  were in good agreement with each  
30 other for the interactions between **2b** and DAO and between TPC and DAO. The  
31 energy decomposition of  $\Delta G_{\text{bind}}$  on a per residue basis calculated that the  
32 contribution of Tyr224 to  $\Delta G_{\text{bind}}$  was greater in the **2b**-DAO interaction than in  
33 the TPC-DAO interaction. We found a notable difference in  $\Delta G_{\text{vdw}, \text{Y224}}$  between

1 the **2b**-DAO and TPC-DAO interactions (**Table 4**). This suggests that Tyr224  
2 contributes to the interaction with low molecular thiophene carboxylic acid-based  
3 inhibitors primarily through hydrophobic interactions.

4 To evaluate the contributions of hydrogen bonds (H-bonds) to the **2b**-DAO  
5 and TPC-DAO interactions, occupancy of each H-bond between molecules  
6 around the active site was calculated (**Fig. 4A**). Characteristic differences  
7 between these interactions were observed in the H-bonds between the inhibitors  
8 and Gly313 and between H<sub>2</sub>O and Tyr224. In the **2b**-DAO complex, a H-bond  
9 network composed of Gln53, Pro54, His217, Tyr224, Gly313 and bridging H<sub>2</sub>O  
10 molecules contributed to stabilization of the S state (**Fig. 4B**). In contrast, a  
11 H-bond network including Tyr224 was not that extensive in the TPC-DAO  
12 complex and partly explaining the preferred D state for this complex (**Fig. 4C**).

13 Taken together the MM/GBSA and H-bond analyses suggest that the  
14 **2b**-Tyr224 interaction and formation of the H-bond network around Tyr224 were  
15 driving forces to form the S state. This was supported by a finding that Tyr224  
16 underwent the largest conformational change among the inhibitor-interacting  
17 residues in the comparison of the structures of the S and D states (**Fig. 5A**).  
18 Leu51 and His217 also changed their conformations as a result of direct  
19 interactions with the inhibitors but to a lesser extent. Although the extent of  
20 conformational changes of Tyr55 and Ile223 appeared significant, these  
21 changes were indirectly influenced by the binding of the inhibitors. Consequently,  
22 Loop 216–228 (referred to as the lid) and Loop 53-62 approached each other in  
23 the **1c**-DAO and **2b** -DAO complexes. These structural changes were  
24 accompanied by a closing of a cleft between the lid and Loop 53-62 to sequester  
25 the substrate binding pocket from the surrounding environment (**Fig. 5B**). In  
26 contrast, the cleft is half-open with the lid relaxed in the TPC-DAO complex, in  
27 which water molecules can pass through from the inside of the pocket to the  
28 surrounding environment (**Fig. 5C**).

29 As a result of the closing of the cleft, the substrate-binding pockets of the  
30 **1c**-DAO and **2b**-DAO complexes appeared to shrink compared with the  
31 complexes in the D state including the TPC-DAO complex (**Tables 5 and 6**).  
32 The extent of shrinkage was the greatest in the **2b**-DAO complex. In addition,  
33 comparison between the averages throughout MD trajectories also indicated a



1 greater extent of shrinkage in the **2b**-DAO complex than in the TPC-DAO  
2 complex.

3

### 4 **3. Discussion**

5 The highly potent DAO/DAAO inhibitors **1c** and **2b** derived from the  
6 thiophene-2-carboxylic acid and thiophene-3-carboxylic acid scaffolds,  
7 respectively, allowed us to investigate the structural basis for the potent DAO  
8 inhibition achieved by such small molecules. Crystal structures and MD analysis  
9 of DAO in complex with the thiophene-based inhibitors suggested that the  
10 complexes prefer the S state and that the formation of the S state is driven by  
11 direct interactions of Tyr224 with the inhibitors and H<sub>2</sub>O. In contrast, the D state  
12 was preferred in the TPC-DAO complex during our MD simulations as shown in  
13 the crystal structure [22]. Given that the D state is preferred by TPC despite the  
14 lack of a side chain, it is conceivable that the core scaffold rather than the  
15 presence or absence of a branched side chain dictates whether the S or D state  
16 is adopted. Further evidence supporting this notion is co-crystal structures of  
17 DAO with 3-hydroxypyridin-2(1H)-one (PDB code: 3w4i) [23]. Even though the  
18 unsubstituted 3-hydroxypyridin-2(1H)-one is small enough to fit into the active  
19 site of the S state structure, the co-crystal structure adopts the D state with a  
20 vacant secondary pocket. One notable structural difference between S and D  
21 state-inducing inhibitors is the presence/absence of a hydrogen bond donor that  
22 can interact with the carbonyl oxygen of Gly313 [23]. In addition, an additional  
23 MD run with a virtual complex in which **2c** was substituted for **2b** in the **2b**-DAO  
24 complex preferred the S state (**Supplementary Fig. 6**), supporting the notion  
25 that the scaffold dictates whether the S or D state is adopted. The precise  
26 mechanism by which DAO adopts the S or D state needs further investigation.

27 The energy decomposition of  $\Delta G_{\text{bind}}$  indicated that the hydrophobic  
28 interaction of **2b**-Tyr224 was stronger than that of TPC-Tyr224. In addition, the  
29 substitution of a halogen for a methyl moiety in the thiophene ring showed  
30 increased potency. These suggested that the  $\pi$ - $\pi$  interaction plays a role in the  
31 interaction between Tyr224 and thiophene-based inhibitors. The side chain of  
32 Tyr224 is electron-donating [27]. Thus, it is inferred that the substitution of a

1 halogen increased potency because the LUMO level of the thiophene ring  
2 decreased due to electron-withdrawing effect of the halogen.

3 A number of scaffolds that promote the formation of the D state have been  
4 published to date. Many of these inhibitors showed potent inhibitory activity by  
5 exploiting the secondary pocket with a large branched chain in combination with  
6 a H-bond with Gly313 [22-24]. In contrast, our thiophene-based inhibitors  
7 including **1c** and **2b** showed low nanomolar inhibitory potency without relying on  
8 the secondary pocket and H-bond with Gly313, but instead by forming a strong  
9 stacking interaction with Tyr224. Indeed, the cleft between the lid and Loop  
10 53-62 was tightly closed in our S state structures, presenting a sharp contrast to  
11 the D state structures accommodating the half-open cleft. Moreover, a H-bond  
12 network including Tyr224 and H<sub>2</sub>O was shown to be extensive in the S state  
13 contributing to the closing of the cleft. It appears difficult to accommodate a large  
14 branched chain in the S state in which the cleft is closed due to the loss of the  
15 secondary pocket. This accounts for the substantial loss of potency caused by  
16 the introduction of a large branched chain to the thiophene ring of either the  
17 2-carboxylic acid or the 3-carboxylic acid scaffolds.

#### 19 **4. Conclusions**

20 Taken together, the present results suggest that the formation of the S state  
21 is driven by the concerted action of the residues around the cleft including  
22 Tyr224 and thiophene carboxylic acid scaffolds in alliance with solvent  
23 molecules. The mechanism by which the thiophene-based inhibitors achieve  
24 potent DAO inhibition is distinct from that of the D-state promoting inhibitors  
25 which exploit the secondary pocket. These findings collectively highlight two  
26 distinct structural optimization approaches to DAO inhibitors depending on how  
27 a given pharmacophore affects the position of Tyr224. For those inducing the S  
28 state, as seen with **1a** and **2a**, the addition of a branched chain unlikely results in  
29 improvement of inhibitory potency. The primary focus of the structural  
30 optimization strategy should be to preserve the S state by avoiding sterically  
31 hindered substituents. On the other hand, pharmacophores promoting the D  
32 state can take full advantage of the secondary pocket generated by the  
33 movement of Tyr224 by incorporating a branched chain. These insights should

1 be of particular importance in future efforts to optimize DAO inhibitors with novel  
2 scaffolds.

## 3 4 **5. Experimental section**

### 5 **5.1. Chemistry**

6 All solvents were reagent grade or HPLC grade. Melting points were  
7 obtained on a Mel-Temp apparatus and are uncorrected. <sup>1</sup>H NMR spectra were  
8 recorded at 400 MHz. The HPLC solvent system consisted of distilled water and  
9 acetonitrile, both containing 0.1% formic acid. Preparative HPLC purification was  
10 performed on an Agilent 1200 Series HPLC system equipped with an Agilent  
11 G1315D DAD detector using a Phenomenex Luna 5 μm C18 (2) column (21.2  
12 mm × 250 mm, 5 μm) with a gradient of 40% ACN/60% H<sub>2</sub>O for 5 minutes  
13 followed by an increase to 100% ACN/0% H<sub>2</sub>O over 40 minutes and a  
14 continuation of 100% ACN/0% H<sub>2</sub>O until 50 minutes at a flow rate of 15 mL/min.  
15 Analytical HPLC was performed on an Agilent 1200 Series HPLC system  
16 equipped with an Agilent G1315D DAD detector (detection at 220 nm), and an  
17 Agilent Quadrupole 6120 LC-MS with electrospray ionization (ESI) source. The  
18 analytical HPLC conditions involve a gradient of 20% ACN/80% H<sub>2</sub>O for 0.25  
19 minutes followed by an increase to 85% ACN/15% H<sub>2</sub>O over 1.75 minutes and  
20 continuation of 85% ACN/15% H<sub>2</sub>O until 4 minutes (detection at 220 nm) with a  
21 Luna C18 column (2.1 mm × 50 mm, 3.5 μm) at a flow rate of 0.75 mL/min. All  
22 final compounds tested were confirmed to be of ≥95% purity by the HPLC  
23 methods described above. Compounds **1a**, **1c-e**, **1i**, **1o**, and **2d** were purchased  
24 from Aldrich. Compounds **1b** and **2b** were purchased from Ark Pharma, Inc.  
25 Compound **1g** was purchased from Enamine. Compounds **1h** and **1r** were  
26 purchased from TCI America. Compounds **1m** and **1q** were purchased from Alfa  
27 Aesar. Compounds **1n** and **1p** were purchased from Parkway Scientific and  
28 ASDI, Inc., respectively. Compounds **2a**, **2c**, and **1s** were purchased from Matrix  
29 Scientific. Compound **1t** and **2e** were purchased from Oakwood Chemical and  
30 Chembridge, respectively. Synthesis of compounds **1f** [28], **1k** [29], **1l** [30], and  
31 **1v** [31] were previously reported.

#### 32 **5.1.1. Synthesis of 4-(difluoromethyl)thiophene-2-carboxylic acid (1j).**

1 To a solution of methyl 4-formylthiophene-2-carboxylate **3** (0.18 g, 1.06  
2 mmol) in dichloromethane (7 mL) at rt was added deoxo-fluor (0.27 g, 1.22  
3 mmol) via syringe. After 4 h of stirring, the reaction was quenched by a careful  
4 addition of sat. NaHCO<sub>3</sub>. The compound was extracted twice with  
5 dichloromethane. The combined organic layers was dried over sodium sulfate  
6 and concentrated to give an oil which was purified by silica gel column (eluent:  
7 10% EtOAc in hexanes) to afford 0.075 g (37% yield) of methyl  
8 4-(difluoromethyl)thiophene-2-carboxylate **4** as a colorless oil. To a solution of **4**  
9 (0.07 g, 0.36 mmol) in a 1:1 mixture of dioxane and water (4 mL) was added 1 N  
10 aqueous solution of sodium hydroxide (1 mL). The reaction was heated at  
11 100 °C for 1 h. Upon completion, the reaction mixture was concentrated in vacuo.  
12 The resulting material was acidified with aqueous 10% KHSO<sub>4</sub> solution to pH~4.  
13 The product was extracted with EtOAc. The organic layer was washed with brine,  
14 dried over Na<sub>2</sub>SO<sub>4</sub>, and concentrated to give 0.065 g (quantitative yield from **4**)  
15 of 4-(difluoromethyl)thiophene-2-carboxylic acid **1j** as a light yellow solid; mp  
16 102 °C. <sup>1</sup>H NMR (CDCl<sub>3</sub>) δ 6.56 (t, *J* = 56.3 Hz, 1H), 7.85 (m, 1H), 7.97 (m, 1H).  
17 LCMS: retention time 1.58 min, *m/z* 179.1 [M + H]<sup>+</sup>.

### 18 **5.1.2. Synthesis of 5-phenethylthiophene-2-carboxylic acid (1u)**

19 To a solution of methyl 5-bromothiophene-2-carboxylate **5u** (0.45 g, 2.04  
20 mmol) in diisopropylamine (10 mL) were added triphenylphosphine (0.21 g, 0.80  
21 mmol), Pd(PhCN)<sub>2</sub>Cl<sub>2</sub> (0.15 g, 0.39 mmol) and copper (I) iodide (0.076 g, 0.40  
22 mmol). Phenylacetylene (0.4 g, 3.92 mmol) was then added under N<sub>2</sub> and the  
23 reaction was heated at 70 °C for 72 h. After cooling to rt, the reaction mixture  
24 was concentrated in vacuo and the residual material was purified by flash  
25 chromatography (eluent: 5% EtOAc/hexanes) to give 0.39 g (79% yield) of  
26 methyl 5-(phenylethynyl)thiophene-2-carboxylate **6u** as a tan solid. <sup>1</sup>H NMR  
27 (CDCl<sub>3</sub>) δ 3.92 (s, 3H), 7.24 (d, *J* = 3.8 Hz, 1H), 7.39-7.40 (m, 3H), 7.54 (m, 2H),  
28 7.71 (d, *J* = 4.0 Hz, 1H). To a solution of **6u** (0.39 g, 1.61 mmol) in EtOAc (50  
29 mL) was added a spatula tip of 10% Pd/C and the mixture was shaken under  
30 hydrogen (50 psi) for 2 h. The catalyst was removed by filtration through a pad of  
31 celite and the filtrate was concentrated to give 0.33 g (83% yield) of methyl  
32 5-(phenylethynyl)thiophene-2-carboxylate **7u** as a yellow oil. <sup>1</sup>H NMR (CDCl<sub>3</sub>) δ  
33 3.00 (t, *J* = 7.3 Hz, 2H), 3.15 (t, *J* = 8.1 Hz, 2H), 3.88 (s, 3H), 6.76 (dt, *J* = 0.8, 3.5

1 Hz, 1H), 7.19 (d,  $J = 7.3$  Hz, 2H), 7.24 (m, 1H), 7.30 (m, 2H), 7.63 (d,  $J = 3.8$  Hz,  
2 1H). To a solution of **7u** (0.33 g, 1.34 mmol) in a 1:1 mixture of water and  
3 methanol (15 mL) was added lithium hydroxide (0.080 g, 3.33 mmol) and the  
4 reaction was heated at 40 °C for 19 h. After completion of the reaction, the  
5 reaction mixture was concentrated in vacuo. The resulting material was acidified  
6 with 1N HCl to pH~2 and the resulting precipitate was filtered to give 0.29 g  
7 (93% yield) of 5-phenethylthiophene-2-carboxylic acid (**1u**) as an off white solid;  
8 mp 114 °C.  $^1\text{H NMR}$  ( $\text{CDCl}_3$ )  $\delta$  3.01 (t,  $J = 7.3$  Hz, 2H), 3.18 (t,  $J = 8.1$  Hz, 2H),  
9 6.80 (dt,  $J = 0.8, 3.8$  Hz, 1H), 7.19-7.22 (m, 2H), 7.24 (m, 1H), 7.30 (m, 2H), 7.72  
10 (d,  $J = 3.8$  Hz, 1H). LCMS: retention time 2.63 min,  $m/z$  233.1  $[\text{M} + \text{H}]^+$ .

### 11 **5.1.3. Synthesis of 4-Phenethylthiophene-2-carboxylic acid (1w).**

12 Methyl 4-(phenylethynyl)thiophene-2-carboxylate **6w** was prepared as  
13 described for the preparation of methyl  
14 5-(phenylethynyl)thiophene-2-carboxylate **6u** except methyl  
15 4-bromothiophene-2-carboxylate **5w** was used in place of methyl  
16 5-bromothiophene-2-carboxylate **5u** and the reaction was heated at 70 °C for 18  
17 h; brown oil (38% yield).  $^1\text{H NMR}$  ( $\text{CDCl}_3$ )  $\delta$  3.93 (s, 3H), 7.37-7.39 (m, 3H),  
18 7.52-7.54 (m, 2H), 7.70 (d,  $J = 1.3$  Hz, 1H), 7.88 (d,  $J = 1.3$  Hz, 1H). Methyl  
19 4-phenethylthiophene-2-carboxylate (**7w**) was prepared as described for the  
20 preparation of methyl 5-phenethylthiophene-2-carboxylate (**7u**) except methyl  
21 4-(phenylethynyl)thiophene-2-carboxylate **6w** was used in place of methyl  
22 5-(phenylethynyl)thiophene-2-carboxylate **6u** and that the mixture was  
23 hydrogenated for 1 h at 40 psi; yellow oil (93% yield).  $^1\text{H NMR}$  ( $\text{CDCl}_3$ )  $\delta$  2.92 (s,  
24 4H), 3.88 (s, 3H), 7.10 (d,  $J = 1.5$  Hz, 1H), 7.14 (m, 2H), 7.20 (m, 1H), 7.28 (m,  
25 2H), 7.65 (d,  $J = 1.5$  Hz, 1H). To a solution of **7w** (0.17 g, 0.69 mmol) in 1:1  
26 mixture of 1,4-dioxane and water (4 mL) was added 1 N aqueous solution of  
27 sodium hydroxide (2.1 mL) and the reaction was heated for 1 h at 100 °C. Upon  
28 completion, the reaction was concentrated in vacuo. The resulting material was  
29 acidified with aqueous 10%  $\text{KHSO}_4$  solution to pH~4. The product was extracted  
30 with EtOAc, washed with brine, dried over  $\text{Na}_2\text{SO}_4$ , and concentrated to give  
31 0.15 g (94% yield) of 4-phenethylthiophene-2-carboxylic acid **1w** as a yellow  
32 solid; mp 136 °C.  $^1\text{H NMR}$  ( $\text{CDCl}_3$ )  $\delta$  2.95 (s, 4H), 7.16-7.24 (m, 4H), 7.28 (m,  
33 2H), 7.72 (d,  $J = 1.5$  Hz, 1H). LCMS: retention time 2.84 min,  $m/z$  233.1  $[\text{M} + \text{H}]^+$ .

**5.1.4. Synthesis of 5-phenethylthiophene-3-carboxylic acid (2f).**

To a solution of 5-bromothiophene-3-carboxylic acid **8** (1.0 g, 4.83 mmol) in acetonitrile (20 mL) was added potassium carbonate (3.3 g, 23.9 mmol) followed by the addition of benzyl bromide (0.63 mL, 5.30 mmol). The mixture was heated at 80 °C for 24 h and concentrated in vacuo. The resulting residue was dissolved in EtOAc and the resulting solution was subsequently washed with water, dried over Na<sub>2</sub>SO<sub>4</sub>, and concentrated to give a light yellow oil. Purification of the crude material by flash chromatography (eluent: 5% EtOAc/hexanes) afforded 0.89 g (62% yield) of benzyl 5-bromothiophene-3-carboxylate (**9**) as a colorless oil. <sup>1</sup>H NMR (CDCl<sub>3</sub>) δ 5.31 (s, 2H), 7.37-7.43 (m, 5H), 7.50 (d, *J* = 1.5 Hz, 1H), 8.03 (d, *J* = 1.5 Hz, 1H). Benzyl 5-(phenylethynyl)thiophene-3-carboxylate **10** was prepared as described for the preparation of methyl 5-(phenylethynyl)thiophene-2-carboxylate **6u** except benzyl 5-bromothiophene-3-carboxylate **9** was used in place of methyl 5-bromothiophene-2-carboxylate **5u** and the reaction was heated at 70 °C for 17 h; brown oil (51% yield). <sup>1</sup>H NMR (CDCl<sub>3</sub>) δ 5.33 (s, 2H), 7.36-7.39 (m, 4H), 7.41-7.46 (m, 4H), 7.69 (d, *J* = 1.3 Hz, 1H), 8.07 (d, *J* = 1.3 Hz, 1H). Benzyl 5-phenethylthiophene-3-carboxylate **11** was prepared as described for the preparation of methyl 5-phenethylthiophene-2-carboxylate **7u** except benzyl 5-(phenylethynyl)thiophene-3-carboxylate **10** was used in place of methyl 5-(phenylethynyl)thiophene-2-carboxylate **6u** and that the mixture was hydrogenated for 1 h at 50 psi; yellow oil (quantitative yield). <sup>1</sup>H NMR (CDCl<sub>3</sub>) δ 2.97 (t, *J* = 7.1 Hz, 2H), 3.10 (t, *J* = 8.6 Hz, 2H), 5.30 (s, 2H), 7.18-7.24 (m, 3H), 7.28 (m, 3H), 7.37-7.45 (m, 5H), 7.94 (d, *J* = 1.3 Hz, 1H). 5-Phenethylthiophene-3-carboxylic acid **2f** was prepared as described for the preparation of compound **1u** except benzyl 5-phenethylthiophene-3-carboxylate **11** was used in place of methyl 5-phenethylthiophene-2-carboxylate **7u** and the reaction was heated in 2:1 mixture of 1,4-dioxane and water at 50 °C for 17 h and the crude material was purified by preparative HPLC; white solid (53% yield); mp 126 °C. <sup>1</sup>H NMR (CDCl<sub>3</sub>) δ 2.99 (t, *J* = 7.1 Hz, 2H), 3.12 (t, *J* = 8.3 Hz, 2H), 7.19-7.24 (m, 3H), 7.29-7.33 (m, 3H), 8.02 (d, *J* = 1.5 Hz, 1H). LCMS: retention time 2.85 min, *m/z* 233.1 [M + H]<sup>+</sup>.

33

## 5.2. In vitro DAO assay

D-Serine was purchased from Bachem Biosciences Inc, horse radish peroxidase from Worthington Biochemical Corporation and *o*-phenylenediamine from Pierce Biotechnology, Inc. All other chemicals were obtained from Sigma-Aldrich. A reliable 96-well plate D-amino acid oxidase (DAO/DAAO) assay was developed based on previously published methods [32]. Briefly, D-serine (5 mM) was oxidatively deaminated by human DAO in the presence of molecular oxygen and flavin adenosine dinucleotide (FAD; 10  $\mu$ M), to yield the corresponding  $\alpha$ -keto acid, ammonia and hydrogen peroxide. The resulting hydrogen peroxide was quantified using horseradish peroxidase (0.01 mg/mL) and *o*-phenylenediamine (180  $\mu$ g/mL), which turns yellowish-brown upon oxidation. DAO activity was correlated to the rate formation of the colored product, i.e., rate of change of absorbance at 411 nm. All reactions were carried out for 20 min at room temperature in a 100- $\mu$ L volume in Tris buffer (50 mM, pH 8.5). Additionally, stock solutions and serial dilutions of potential DAO inhibitors were made in 20:80 DMSO:buffer with a final assay DMSO concentration of 2%.

## 5.3. X-ray crystallography

Expression, purification and crystallization of human DAO were previously described [19]. Briefly, full-length DAO protein was expressed using pET11b (Novagen) and *E. coli* BL21 (DE3). After disruption of cells, the extract was centrifuged, heated and fractionated with ammonium sulfate. The sample was applied to DEAE (Sigma-Aldrich) and hydroxylapatite columns (Nacalai). DAO was crystallized with 15% [w/v] PEG 4000, 0.2 M ammonium acetate, 0.1 M Na citrate at pH 8.0, and 10% [v/v] glycerol. **1c** and **2b** (1 mM each) were soaked into the crystals prior to X-ray diffraction experiments. Diffraction data were collected at Photon Factory AR NW12A and SPring-8 BL44XU. Scaling, molecular replacement and model building were performed with iMosfilm [33], XDS [34], MolRep [35] and Coot [36], respectively. Refinement was performed as previously described using Refmac and Phenix [37-39].

## 5.4. Molecular dynamics

Dimer structures of the complexes of **2b**-DAO (PDB code: 5zj9) and

1 TPC-DAO (PDB code: 3znn) retaining cofactors and water molecules were used  
2 as initial structures. The initial structure in the D state with **2b** was constructed by  
3 superimposing 3znn and 5zj9 and subsequently combining the coordinates of **2b**  
4 with the 3znn coordinates without TPC. The construction of the initial structure in  
5 the S state with TPC and **2c** followed a similar procedure. Structure optimization  
6 and calculation of electrostatic potentials of ligands were performed with the  
7 HF/6-31G(d) basis set using Gaussian 09 [40]. Atomic charges and atom types  
8 were assigned using Antechamber [41]. Generalized Amber force field (GAFF)  
9 implemented in the LEaP module of the Amber suite was used to parameterize  
10 ligands [42, 43]. Ionization states of charged residues were calculated according  
11 to ProPKA [44]. The Amber ff14SB force field was used for polypeptide chains.  
12 All systems were solvated in TIP3P water boxes with the minimum margin of 10  
13 Å using solvate1.0 and the LEaP module [45]. Cl<sup>-</sup> was added to neutralize the  
14 systems. Na<sup>+</sup> and Cl<sup>-</sup> were further added to adjust the salt concentration of the  
15 systems to 0.15 M.

16 Energy minimization was performed using Amber 14 with 10-Å cut-off for the  
17 non-bonded interactions [43]. 5000 steps of steepest descent minimization were  
18 performed followed by 5000 steps of conjugate gradient minimization using the  
19 Particle Mesh Ewald method under constant-volume and periodic boundary  
20 conditions. An initial minimization was performed for solvent molecules and  
21 hydrogen atoms followed by minimization for all atoms in the systems.

22 The systems were gradually heated from 0 to 310 K under constant-volume  
23 conditions. The temperature was controlled using Langevin dynamics with a  
24 collision frequency of 2.0 ps<sup>-1</sup>. Step size was set to 2 fs with fixed bond lengths  
25 involving all hydrogen atoms using the SHAKE algorithm [46]. Motions of all  
26 solute atoms except hydrogens were restricted during the heating process.  
27 Equilibration and production MD simulations were performed under 1 atm at 310  
28 K without motion restrictions for all atoms as previously described [47, 48].  
29 Equilibration of the systems was monitored as shown in **Supplementary Figs.**  
30 **7-11.**

31

## 32 **5.5. Binding free energy calculations**

33 Calculations of binding free energy ( $\Delta G_{\text{bind}}$ ) of inhibitors to DAO were



1 performed by the molecular mechanics energies combined with the generalized  
 2 Born and surface area (MM/GBSA) method implemented in the AmberTools14  
 3 suite [49, 50]. Binding free energy ( $\Delta G_{\text{bind}}$ ) was previously defined as below [48,  
 4 51, 52].

$$5 \quad \Delta G_{\text{bind}} = \Delta G^{\text{MM}} + \Delta G^{\text{solv}} = \Delta H_{\text{bind}} - T\Delta S^{\text{MM}}$$

6 where  $\Delta G^{\text{MM}}$ ,  $\Delta G^{\text{solv}}$ ,  $\Delta H_{\text{bind}}$  and  $T\Delta S^{\text{MM}}$  refer to molecular mechanics free energy,  
 7 solvation free energy, binding enthalpy and entropy term, respectively.

$$8 \quad \Delta G^{\text{MM}} = \Delta E^{\text{MM}} - T\Delta S^{\text{MM}}$$

9 where  $\Delta E^{\text{MM}}$  refers to enthalpy in the gas phase upon complex formation.

$$10 \quad \Delta H_{\text{bind}} = \Delta E^{\text{MM}} + \Delta G^{\text{solv}}$$

$$11 \quad \Delta E^{\text{MM}} = \Delta E_{\text{vdw}} + \Delta E_{\text{elec}}$$

12 where  $\Delta E_{\text{vdw}}$  and  $\Delta E_{\text{elec}}$  refer to van der Waals and electrostatic interaction  
 13 energies, respectively.

$$14 \quad \Delta G^{\text{solv}} = \Delta G_{\text{polar}}^{\text{solv}} + \Delta G_{\text{nonpolar}}^{\text{solv}}$$

15 where  $\Delta G_{\text{polar}}^{\text{solv}}$  and  $\Delta G_{\text{nonpolar}}^{\text{solv}}$  refer to polar and nonpolar contributions of  
 16 solvation free energy, respectively.

17  $\Delta G_{\text{exp}}$  was calculated from the  $\text{IC}_{50}$  using the following relations [51].

$$18 \quad \Delta G_{\text{exp}} = \sim RT \ln \text{IC}_{50}$$

19 Where R and T are the ideal gas constant and absolute temperature,  
 20 respectively.

21  $T\Delta S^{\text{MM}}$  was calculated using the quasi-harmonic approximation [53]. H-bond  
 22 occupancy was calculated using CPPTRAJ implemented in the AmberTools14  
 23 suite [54].

24

## 25 **5.6. Data availability**

26 The atomic coordinates of inhibitor-DAO complexes were deposited in the  
 27 Protein Data Bank. The access codes are 5zja (**1c**-DAO complex) and 5zj9  
 28 (**2b**-DAO complex).

29

30

## 31 **Acknowledgements**

32 This research was supported in part by a grant for Enzyme Research from  
 33 the Japan Foundation for Applied Enzymology, a research grant from the

1 National Institutes of Health (R01MH091387) and JSPS KAKENHI Grant  
2 Number 18K06580. We thank the beamline staff at the Photon Factory (proposal  
3 No: 2013G075) and the SPring-8 BL44XU (Proposal No. 2015A6537  
4 and 2015B6537) for supporting the data collection. Authors declare no conflict of  
5 interests.

6

7

## 8 **Appendix A. Supplementary data**

9 Supplementary data related to this article can be found at

10

11

## 12 **Figure legends**

13

### 14 **Fig 1 Structural change of Tyr224 in response to bound inhibitors**

15 A, C: Tyr224 in the S state. In the complex structure of **2b**-DAO, Tyr224 (yellow)  
16 is stacked with the thiophene ring of the inhibitor. The secondary pocket is lost in  
17 this state.

18 B, D: Tyr224 in the D state. In the complex structure between CPC and DAO, the  
19 side chain of Tyr224 is shifted to allow an additional pocket (i.e. the secondary  
20 pocket) to appear, which accommodates the branched side chain of the inhibitor  
21 [22](PDB code: 3zno). A yellow dashed circle indicates the secondary pocket.  
22 The structure and IC<sub>50</sub> value of CPC are shown in **Supplementary Table 2**.

23

### 24 **Fig 2 The active sites of the 1c-DAO and 2b-DAO complexes**

25 A: The active site of the crystal structure of the **1c**-DAO complex

26 B: The active site of the crystal structure of the **2b**-DAO complex

27 C: Superimposition of the **1c**-DAO (pale cyan) and **2b**-DAO (yellow) complexes

28

### 29 **Fig 3 Distance between the benzene ring of Tyr224 and the 5-membered** 30 **rings of the DAO inhibitors**

31 All panels in this figure indicate the results for Chain A of DAO dimers. The  
32 results for Chain B are shown in **Supplementary Figs. 1-4**. On top of the panels,  
33 initial and final states under individual simulation conditions are illustrated. An

1 arrowhead in each panel indicates the distance between the centroids of the  
2 rings of Tyr224 and inhibitors in the initial structure.  
3 A: Distance between the centroids of the rings of Tyr224 and **2b** during a MD  
4 simulation. The initial structure for this run was a dimer crystal structure of the  
5 **2b**-DAO complex, which is in the S state. The average distance between the  
6 centroids throughout trajectories was 4.04 Å.  
7 B: Distance between the centroids of the benzene ring of Tyr224 and pyrrole ring  
8 of TPC during a MD simulation. The initial structure for this run was a dimer  
9 crystal structure of the TPC-DAO complex, which is in the D state. The structure  
10 and IC<sub>50</sub> value of TPC are shown in **Supplementary Table 2**.  
11 C: Distance between the centroids of the rings of Tyr224 and **2b** during a MD  
12 simulation. The initial structure for this run was a hypothetical structure in which  
13 a D state structure of DAO derived from the TPC-DAO complex structure was  
14 combined with the coordinates of **2b**.  
15 D: Distance between the centroids of the rings of Tyr224 and TPC during a MD  
16 simulation. The initial structure for this run was a hypothetical structure in which  
17 an S state structure of DAO derived from the **2b**-DAO complex structure was  
18 combined with the coordinates of TPC.

19

#### 20 **Fig 4 Analysis of H-bond networks around the active site**

21 A: Occupancy of H-bonds between inhibitors and DAO (left) and between H<sub>2</sub>O  
22 and DAO (right). The listed H-bonds between H<sub>2</sub>O and DAO are those bridging  
23 Tyr224 and other DAO residues via H<sub>2</sub>O.

24 B: H-bond networks around the active site in the **2b**-DAO complex depicted  
25 based on Panel A (Occupancy > 0.4). Cyan lines and red balls indicate H-bonds  
26 and oxygen atoms of H<sub>2</sub>O molecules, respectively.

27 C: H-bond networks around the active site in the TPC-DAO complex depicted  
28 based on Panel A (Occupancy > 0.4).

29

#### 30 **Fig 5 Difference of S and D state structures**

31 A: Loops around the active sites of superimposed DAO structures in complex  
32 with **2b** (pale cyan) and TPC (yellow).

33 B: The **2b**-DAO complex viewed from the surface of the protein molecule.

1 Orange spheres and blue balls indicate **2b** and oxygen atoms of H<sub>2</sub>O,  
2 respectively. Transparent surface in pale cyan corresponds to the lid and Loop  
3 53-62.

4 C: The TPC-DAO complex viewed from the surface of the protein molecule.  
5 Orange spheres and blue balls indicate TPC and oxygen atoms of H<sub>2</sub>O,  
6 respectively. Transparent surface in yellow corresponds to the lid and Loop  
7 53-62.

8

9

## 10 **References**

11 [1] Y. Kato, D.H. Tran, H.T.T. Trinh, K. Fukui, D-Amino Acid Oxidase and  
12 D-Aspartate Oxidase., in: T. Yoshimura, T. Nishikawa, H. Homma (Eds.)  
13 D-amino acids : physiology, metabolism, and application, Springer, Japan,  
14 2016, pp. 293-309.

15 [2] A. Hashimoto, T. Nishikawa, T. Oka, K. Takahashi, Endogenous D-serine  
16 in rat brain: N-methyl-D-aspartate receptor-related distribution and aging,  
17 *Journal of neurochemistry*, 60 (1993) 783-786.

18 [3] J.P. Mothet, A.T. Parent, H. Wolosker, R.O. Brady, Jr., D.J. Linden, C.D.  
19 Ferris, M.A. Rogawski, S.H. Snyder, D-serine is an endogenous ligand for the  
20 glycine site of the N-methyl-D-aspartate receptor, *Proceedings of the*  
21 *National Academy of Sciences of the United States of America*, 97 (2000)  
22 4926-4931.

23 [4] M.J. Schell, M.E. Molliver, S.H. Snyder, D-serine, an endogenous  
24 synaptic modulator: localization to astrocytes and glutamate-stimulated  
25 release, *Proceedings of the National Academy of Sciences of the United*  
26 *States of America*, 92 (1995) 3948-3952.

27 [5] P.W. Burnet, S.L. Eastwood, G.C. Bristow, B.R. Godlewska, P. Sikka, M.  
28 Walker, P.J. Harrison, D-amino acid oxidase activity and expression are  
29 increased in schizophrenia, *Molecular psychiatry*, 13 (2008) 658-660.

30 [6] K. Ono, Y. Shishido, H.K. Park, T. Kawazoe, S. Iwana, S.P. Chung, R.M.  
31 Abou El-Magd, K. Yorita, M. Okano, T. Watanabe, N. Sano, Y. Bando, K.  
32 Arima, T. Sakai, K. Fukui, Potential pathophysiological role of D-amino acid  
33 oxidase in schizophrenia: immunohistochemical and in situ hybridization

- 1 study of the expression in human and rat brain, *Journal of neural*  
2 *transmission* (Vienna, Austria : 1996), 116 (2009) 1335-1347.
- 3 [7] K. Hashimoto, T. Fukushima, E. Shimizu, N. Komatsu, H. Watanabe, N.  
4 Shinoda, M. Nakazato, C. Kumakiri, S. Okada, H. Hasegawa, K. Imai, M. Iyo,  
5 Decreased serum levels of D-serine in patients with schizophrenia: evidence  
6 in support of the N-methyl-D-aspartate receptor hypofunction hypothesis of  
7 schizophrenia, *Archives of general psychiatry*, 60 (2003) 572-576.
- 8 [8] M.A. Calcia, C. Madeira, F.V. Alheira, T.C. Silva, F.M. Tannos, C.  
9 Vargas-Lopes, N. Goldenstein, M.A. Brasil, S.T. Ferreira, R. Panizzutti,  
10 Plasma levels of D-serine in Brazilian individuals with schizophrenia,  
11 *Schizophrenia research*, 142 (2012) 83-87.
- 12 [9] T. Fukushima, H. Iizuka, A. Yokota, T. Suzuki, C. Ohno, Y. Kono, M.  
13 Nishikiori, A. Seki, H. Ichiba, Y. Watanabe, S. Hongo, M. Utsunomiya, M.  
14 Nakatani, K. Sadamoto, T. Yoshio, Quantitative analyses of  
15 schizophrenia-associated metabolites in serum: serum D-lactate levels are  
16 negatively correlated with gamma-glutamylcysteine in medicated  
17 schizophrenia patients, *PloS one*, 9 (2014) e101652.
- 18 [10] K. Hashimoto, G. Engberg, E. Shimizu, C. Nordin, L.H. Lindstrom, M.  
19 Iyo, Reduced D-serine to total serine ratio in the cerebrospinal fluid of drug  
20 naive schizophrenic patients, *Progress in neuro-psychopharmacology &*  
21 *biological psychiatry*, 29 (2005) 767-769.
- 22 [11] D.C. Goff, M. Hill, D. Barch, The treatment of cognitive impairment in  
23 schizophrenia, *Pharmacology, biochemistry, and behavior*, 99 (2011)  
24 245-253.
- 25 [12] D. Cadinu, B. Grayson, G. Podda, M.K. Harte, N. Doostdar, J.C. Neill,  
26 NMDA receptor antagonist rodent models for cognition in schizophrenia and  
27 identification of novel drug treatments, an update, *Neuropharmacology*,  
28 (2017).
- 29 [13] H.Y. Lane, C.H. Lin, M.F. Green, G. Helleman, C.C. Huang, P.W. Chen,  
30 R. Tun, Y.C. Chang, G.E. Tsai, Add-on treatment of benzoate for  
31 schizophrenia: a randomized, double-blind, placebo-controlled trial of  
32 D-amino acid oxidase inhibitor, *JAMA psychiatry*, 70 (2013) 1267-1275.
- 33 [14] D.V. Ferraris, T. Tsukamoto, Recent advances in the discovery of

- 1 D-amino acid oxidase inhibitors and their therapeutic utility in  
2 schizophrenia, *Current pharmaceutical design*, 17 (2011) 103-111.
- 3 [15] G. Molla, Competitive Inhibitors Unveil Structure/Function  
4 Relationships in Human D-Amino Acid Oxidase, *Frontiers in molecular*  
5 *biosciences*, 4 (2017) 80.
- 6 [16] R. Konno, S. Uchiyama, Y. Yasumura, Intraspecies and interspecies  
7 variations in the substrate specificity of D-amino acid oxidase, *Comparative*  
8 *biochemistry and physiology. B, Comparative biochemistry*, 71 (1982)  
9 735-738.
- 10 [17] C. Setoyama, Y. Nishina, H. Mizutani, I. Miyahara, K. Hirotsu, N.  
11 Kamiya, K. Shiga, R. Miura, Engineering the substrate specificity of porcine  
12 kidney D-amino acid oxidase by mutagenesis of the "active-site lid", *Journal*  
13 *of biochemistry*, 139 (2006) 873-879.
- 14 [18] R. Miura, C. Setoyama, Y. Nishina, K. Shiga, H. Mizutani, I. Miyahara,  
15 K. Hirotsu, Structural and mechanistic studies on D-amino acid oxidase x  
16 substrate complex: implications of the crystal structure of enzyme x  
17 substrate analog complex, *Journal of biochemistry*, 122 (1997) 825-833.
- 18 [19] T. Kawazoe, H. Tsuge, M.S. Pilone, K. Fukui, Crystal structure of  
19 human D-amino acid oxidase: context-dependent variability of the backbone  
20 conformation of the VAAGL hydrophobic stretch located at the si-face of the  
21 flavin ring, *Protein science : a publication of the Protein Society*, 15 (2006)  
22 2708-2717.
- 23 [20] A. Mattevi, M.A. Vanoni, F. Todone, M. Rizzi, A. Teplyakov, A. Coda, M.  
24 Bolognesi, B. Curti, Crystal structure of D-amino acid oxidase: a case of  
25 active site mirror-image convergent evolution with flavocytochrome b2,  
26 *Proceedings of the National Academy of Sciences of the United States of*  
27 *America*, 93 (1996) 7496-7501.
- 28 [21] T. Kawazoe, H. Tsuge, T. Imagawa, K. Aki, S. Kuramitsu, K. Fukui,  
29 Structural basis of D-DOPA oxidation by D-amino acid oxidase: alternative  
30 pathway for dopamine biosynthesis, *Biochemical and biophysical research*  
31 *communications*, 355 (2007) 385-391.
- 32 [22] S.C. Hopkins, M.L. Heffernan, L.D. Saraswat, C.A. Bowen, L. Melnick,  
33 L.W. Hardy, M.A. Orsini, M.S. Allen, P. Koch, K.L. Spear, R.J. Foglesong, M.

- 1 Soukri, M. Chytil, Q.K. Fang, S.W. Jones, M.A. Varney, A. Panatier, S.H.  
2 Oliet, L. Pollegioni, L. Piubelli, G. Molla, M. Nardini, T.H. Large, Structural,  
3 kinetic, and pharmacodynamic mechanisms of D-amino acid oxidase  
4 inhibition by small molecules, *Journal of medicinal chemistry*, 56 (2013)  
5 3710-3724.
- 6 [23] T. Hondo, M. Warizaya, T. Niimi, I. Namatame, T. Yamaguchi, K.  
7 Nakanishi, T. Hamajima, K. Harada, H. Sakashita, Y. Matsumoto, M. Orita,  
8 M. Takeuchi, 4-Hydroxypyridazin-3(2H)-one derivatives as novel D-amino  
9 acid oxidase inhibitors, *Journal of medicinal chemistry*, 56 (2013) 3582-3592.
- 10 [24] N. Hin, B. Duvall, D. Ferraris, J. Alt, A.G. Thomas, R. Rais, C. Rojas, Y.  
11 Wu, K.M. Wozniak, B.S. Slusher, T. Tsukamoto,  
12 6-Hydroxy-1,2,4-triazine-3,5(2H,4H)-dione Derivatives as Novel D-Amino  
13 Acid Oxidase Inhibitors, *Journal of medicinal chemistry*, 58 (2015)  
14 7258-7272.
- 15 [25] M. Katane, N. Osaka, S. Matsuda, K. Maeda, T. Kawata, Y. Saitoh, M.  
16 Sekine, T. Furuchi, I. Doi, S. Hirono, H. Homma, Identification of novel  
17 D-amino acid oxidase inhibitors by in silico screening and their functional  
18 characterization in vitro, *Journal of medicinal chemistry*, 56 (2013)  
19 1894-1907.
- 20 [26] T. Sparey, P. Abeywickrema, S. Almond, N. Brandon, N. Byrne, A.  
21 Campbell, P.H. Hutson, M. Jacobson, B. Jones, S. Munshi, D. Pascarella, A.  
22 Pike, G.S. Prasad, N. Sachs, M. Sakatis, V. Sardana, S. Venkatraman, M.B.  
23 Young, The discovery of fused pyrrole carboxylic acids as novel, potent  
24 D-amino acid oxidase (DAO) inhibitors, *Bioorganic & medicinal chemistry*  
25 *letters*, 18 (2008) 3386-3391.
- 26 [27] M.L. Fonda, B.M. Anderson, D-amino acid oxidase. II. Studies of  
27 substrate-competitive inhibitors, *The Journal of biological chemistry*, 243  
28 (1968) 1931-1935.
- 29 [28] S. Kasai, H. Igawa, M. Takahashi, T. Maekawa, K. Kakegawa, T.  
30 Yasuma, A. Kina, J. Aida, U. Khamrai, M. Kundu, Preparation of  
31 benzimidazole and imidazopyridine derivatives and analogs as MCH  
32 receptor antagonists for treating obesity, in, Takeda Pharmaceutical  
33 Company Limited, Japan . 2013.

- 1 [29] P. Wang, M. Ji, F. Sha, An efficient and facile process for synthesis of  
2 4,5-dichlorothiophene-2-carboxylic acid using N-chlorosuccinimide, *J. Chem.*  
3 *Res.*, 38 (2014) 622-624.
- 4 [30] D.R. Parry, I.R. Matthews, G. Mitchell, A.G. Williams, N.J. Barnes, J.M.  
5 Cox, K.J. Gillen, M.P. Ensminger, K. Khodayari, H. Nakayama, Preparation  
6 of cyclopropylcarbonylaminopyrrolidinones, -thiazolidinones, or  
7 -oxazolidinones as herbicides, in, Zeneca Limited, UK . 2000.
- 8 [31] S. Gronowitz, T. Klingstedt, L. Svensson, U. Hansson, On the syntheses  
9 of branched saturated fatty acids, *Lipids*, 28 (1993) 889-897.
- 10 [32] S.P. Cook, I. Galve-Roperh, A. Martinez del Pozo, I. Rodriguez-Crespo,  
11 Direct calcium binding results in activation of brain serine racemase, *The*  
12 *Journal of biological chemistry*, 277 (2002) 27782-27792.
- 13 [33] T.G. Battye, L. Kontogiannis, O. Johnson, H.R. Powell, A.G. Leslie,  
14 iMOSFLM: a new graphical interface for diffraction-image processing with  
15 MOSFLM, *Acta crystallographica. Section D, Biological crystallography*, 67  
16 (2011) 271-281.
- 17 [34] W. Kabsch, XDS, *Acta crystallographica. Section D, Biological*  
18 *crystallography*, 66 (2010) 125-132.
- 19 [35] A. Vagin, A. Teplyakov, MOLREP: an automated program for molecular  
20 replacement, *J. Appl. Crystallogr.*, 30 (1997) 1022-1025.
- 21 [36] P. Emsley, B. Lohkamp, W.G. Scott, K. Cowtan, Features and  
22 development of Coot, *Acta Crystallogr., Sect. D: Biol. Crystallogr.*, 66 (2010)  
23 486-501.
- 24 [37] G.N. Murshudov, A.A. Vagin, E.J. Dodson, Refinement of  
25 macromolecular structures by the maximum-likelihood method, *Acta*  
26 *Crystallogr., Sect. D: Biol. Crystallogr.*, D53 (1997) 240-255.
- 27 [38] P.D. Adams, P.V. Afonine, G. Bunkoczi, V.B. Chen, I.W. Davis, N.  
28 Echols, J.J. Headd, L.W. Hung, G.J. Kapral, R.W. Grosse-Kunstleve, A.J.  
29 McCoy, N.W. Moriarty, R. Oeffner, R.J. Read, D.C. Richardson, J.S.  
30 Richardson, T.C. Terwilliger, P.H. Zwart, PHENIX: a comprehensive  
31 Python-based system for macromolecular structure solution, *Acta*  
32 *Crystallogr., Sect. D: Biol. Crystallogr.*, 66 (2010) 213-221.
- 33 [39] Y.S. Kato, F. Yumoto, H. Tanaka, T. Miyakawa, Y. Miyauchi, D.



- 1 Takeshita, Y. Sawano, T. Ojima, I. Ohtsuki, M. Tanokura, Structure of the  
2 Ca(2+)-saturated C-terminal domain of scallop troponin C in complex with a  
3 troponin I fragment, *Biological chemistry*, 394 (2013) 55-68.
- 4 [40] M.J. Frisch, G.W. Trucks, H.B. Schlegel, G.E. Scuseria, M.A. Robb, J.R.  
5 Cheeseman, G. Scalmani, V. Barone, G.A. Petersson, H. Nakatsuji, X. Li, M.  
6 Caricato, A. Marenich, J. Bloino, B.G. Janesko, R. Gomperts, B. Mennucci,  
7 H.P. Hratchian, J.V. Ortiz, A.F. Izmaylov, J.L. Sonnenberg, D.  
8 Williams-Young, F. Ding, F. Lipparini, F. Egidi, J. Goings, B. Peng, A.  
9 Petrone, T. Henderson, D. Ranasinghe, V.G. Zakrzewski, J. Gao, N. Rega, G.  
10 Zheng, W. Liang, M. Hada, M. Ehara, K. Toyota, R. Fukuda, J. Hasegawa, M.  
11 Ishida, T. Nakajima, Y. Honda, O. Kitao, H. Nakai, T. Vreven, K. Throssell, J.  
12 Montgomery, J. A., J.E. Peralta, F. Ogliaro, M. Bearpark, J.J. Heyd, E.  
13 Brothers, K.N. Kudin, V.N. Staroverov, T. Keith, R. Kobayashi, J. Normand,  
14 K. Raghavachari, A. Rendell, J.C. Burant, S.S. Iyengar, J. Tomasi, M. Cossi,  
15 J.M. Millam, M. Klene, C. Adamo, R. Cammi, J.W. Ochterski, R.L. Martin, K.  
16 Morokuma, O. Farkas, J.B. Foresman, D.J. Fox, Gaussian 09, Revision A.02,  
17 in, Gaussian, Inc., Wallingford CT, 2016.
- 18 [41] J. Wang, W. Wang, P.A. Kollman, D.A. Case, Automatic atom type and  
19 bond type perception in molecular mechanical calculations, *J. Mol. Graphics*  
20 *Modell.*, 25 (2006) 247-260.
- 21 [42] J. Wang, R.M. Wolf, J.W. Caldwell, P.A. Kollman, D.A. Case,  
22 Development and testing of a general Amber force field, *J. Comput. Chem.*,  
23 25 (2004) 1157-1174.
- 24 [43] D.A. Case, V. Babin, J.T. Berryman, R.M. Betz, Q. Cai, D.S. Cerutti, I.  
25 Cheatham, T.E. , T.A. Darden, R.E. Duke, H. Gohlke, A.W. Goetz, S.  
26 Gusarov, N. Homeyer, P. Janowski, J. Kaus, I. Kolossva□ry, A. Kovalenko,  
27 T.S. Lee, S. LeGrand, T. Luchko, R. Luo, B. Madej, K.M. Merz, F. Paesani,  
28 D.R. Roe, A. Roitberg, C. Sagui, R. Salomon-Ferrer, G. Seabra, C.L.  
29 Simmerling, W. Smith, J. Swails, R.C. Walker, J. Wang, R.M. Wolf, W. X., K.  
30 P.A., Amber 14, in, University of California, San Francisco, 2014.
- 31 [44] M.H.M. Olsson, C.R. Sondergaard, M. Rostkowski, J.H. Jensen,  
32 PROPKA3: Consistent Treatment of Internal and Surface Residues in  
33 Empirical pKa Predictions, *J. Chem. Theory Comput.*, 7 (2011) 525-537.

- 1 [45] H. Grubmüller, V. Goll, SOLVATE1.0, in, University of Munich, 1996.
- 2 [46] J.-P. Ryckaert, G. Ciccotti, H.J.C. Berendsen, Numerical integration of  
3 the cartesian equations of motion of a system with constraints: molecular  
4 dynamics of n-alkanes, *Journal of Computational Physics*, 23 (1977) 327-341.
- 5 [47] Y.S. Kato, T. Yagi, S.A. Harris, S.Y. Ohki, K. Yura, Y. Shimizu, S.  
6 Honda, R. Kamiya, S.A. Burgess, M. Tanokura, Structure of the  
7 microtubule-binding domain of flagellar dynein, *Structure* (London,  
8 England : 1993), 22 (2014) 1628-1638.
- 9 [48] Y. Kato, H. Kihara, K. Fukui, M. Kojima, A ternary complex model of  
10 Sirtuin4-NAD(+)-Glutamate dehydrogenase, *Comput Biol Chem*, 74 (2018)  
11 94-104.
- 12 [49] A. Onufriev, D. Bashford, D.A. Case, Exploring protein native states and  
13 large-scale conformational changes with a modified generalized born model,  
14 *Proteins*, 55 (2004) 383-394.
- 15 [50] B.R. Miller, 3rd, T.D. McGee, Jr., J.M. Swails, N. Homeyer, H. Gohlke,  
16 A.E. Roitberg, MMPBSA.py: An Efficient Program for End-State Free  
17 Energy Calculations, *Journal of chemical theory and computation*, 8 (2012)  
18 3314-3321.
- 19 [51] M. Malaisree, T. Rungrotmongkol, N. Nunthaboot, O. Aruksakunwong,  
20 P. Intharathep, P. Decha, P. Sompornpisut, S. Hannongbua, Source of  
21 oseltamivir resistance in avian influenza H5N1 virus with the H274Y  
22 mutation, *Amino acids*, 37 (2009) 725-732.
- 23 [52] Y. Zou, F. Wang, Y. Wang, W. Guo, Y. Zhang, Q. Xu, Y. Lai, Systematic  
24 study of imidazoles inhibiting IDO1 via the integration of molecular  
25 mechanics and quantum mechanics calculations, *European journal of*  
26 *medicinal chemistry*, 131 (2017) 152-170.
- 27 [53] J. Schlitter, Estimation of absolute and relative entropies of  
28 macromolecules using the covariance matrix, *Chemical Physics Letters*, 215  
29 (1993) 617-621.
- 30 [54] D.R. Roe, T.E. Cheatham, 3rd, PTRAJ and CPPTRAJ: Software for  
31 Processing and Analysis of Molecular Dynamics Trajectory Data, *Journal of*  
32 *chemical theory and computation*, 9 (2013) 3084-3095.

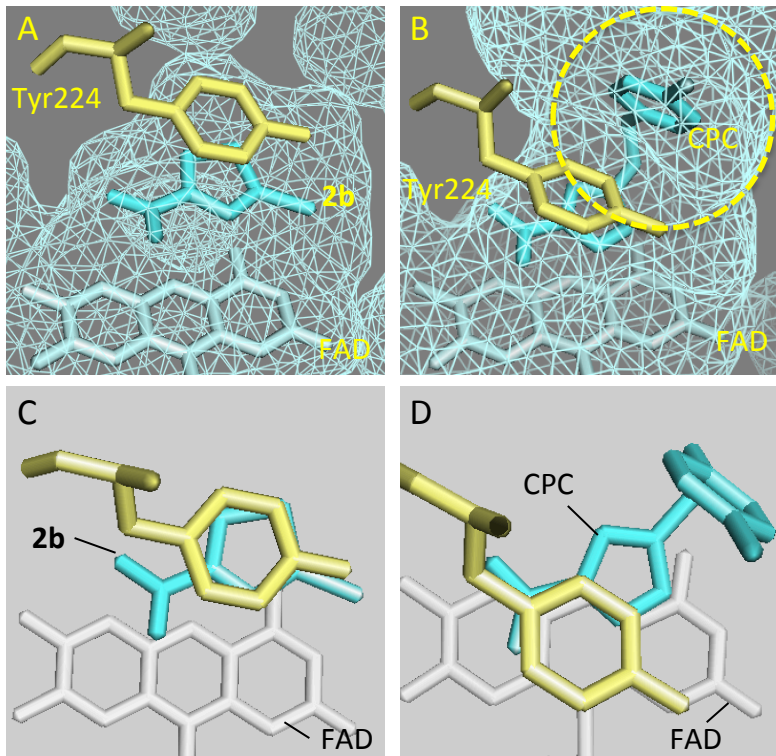


Fig. 1

Kato et al. 2018

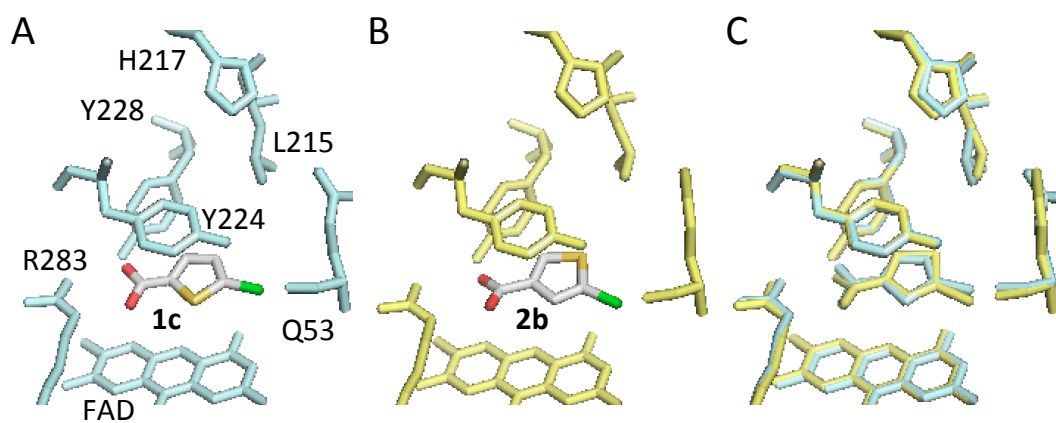


Fig. 2

Kato et al. 2018

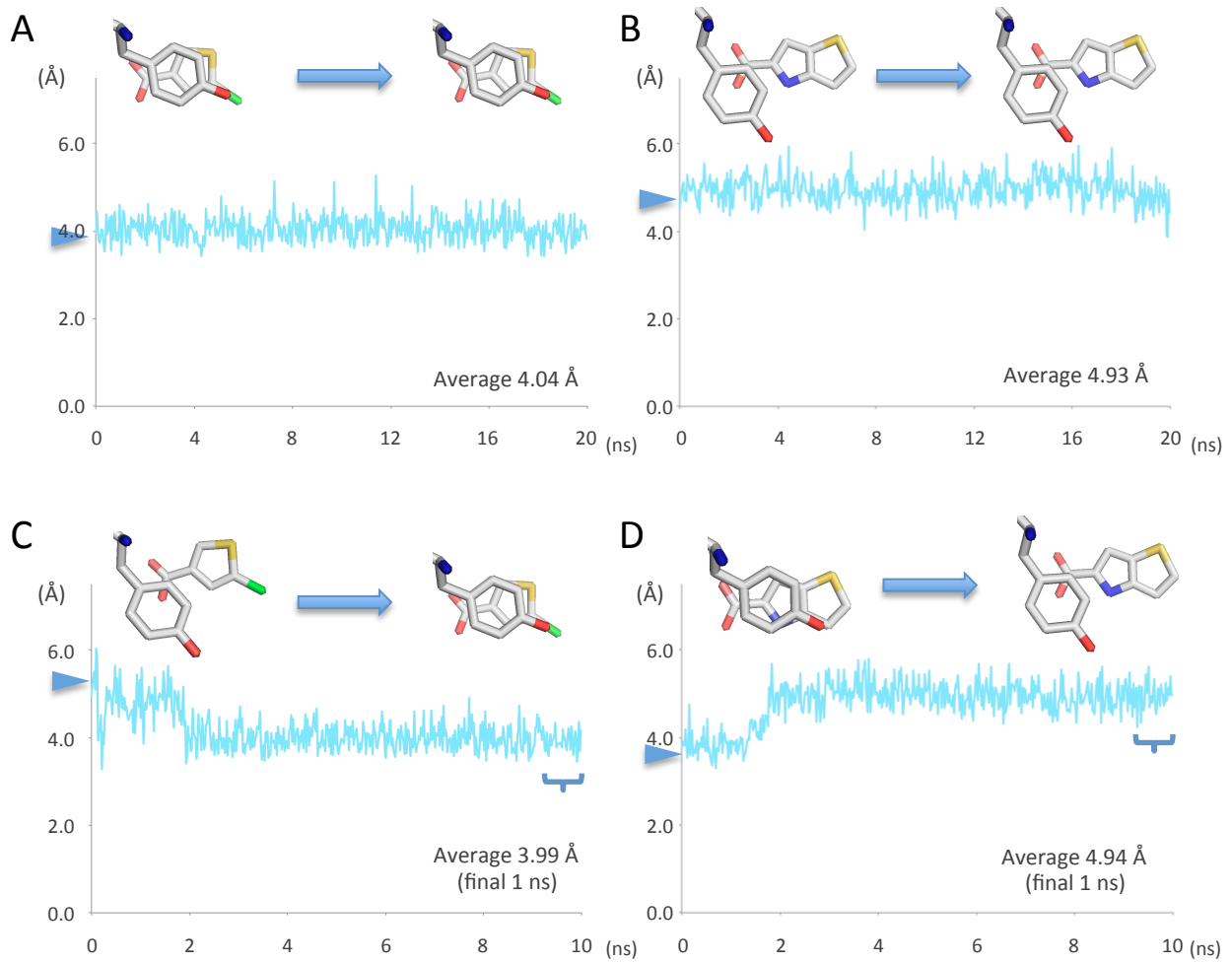


Fig. 3

Kato et al. 2018

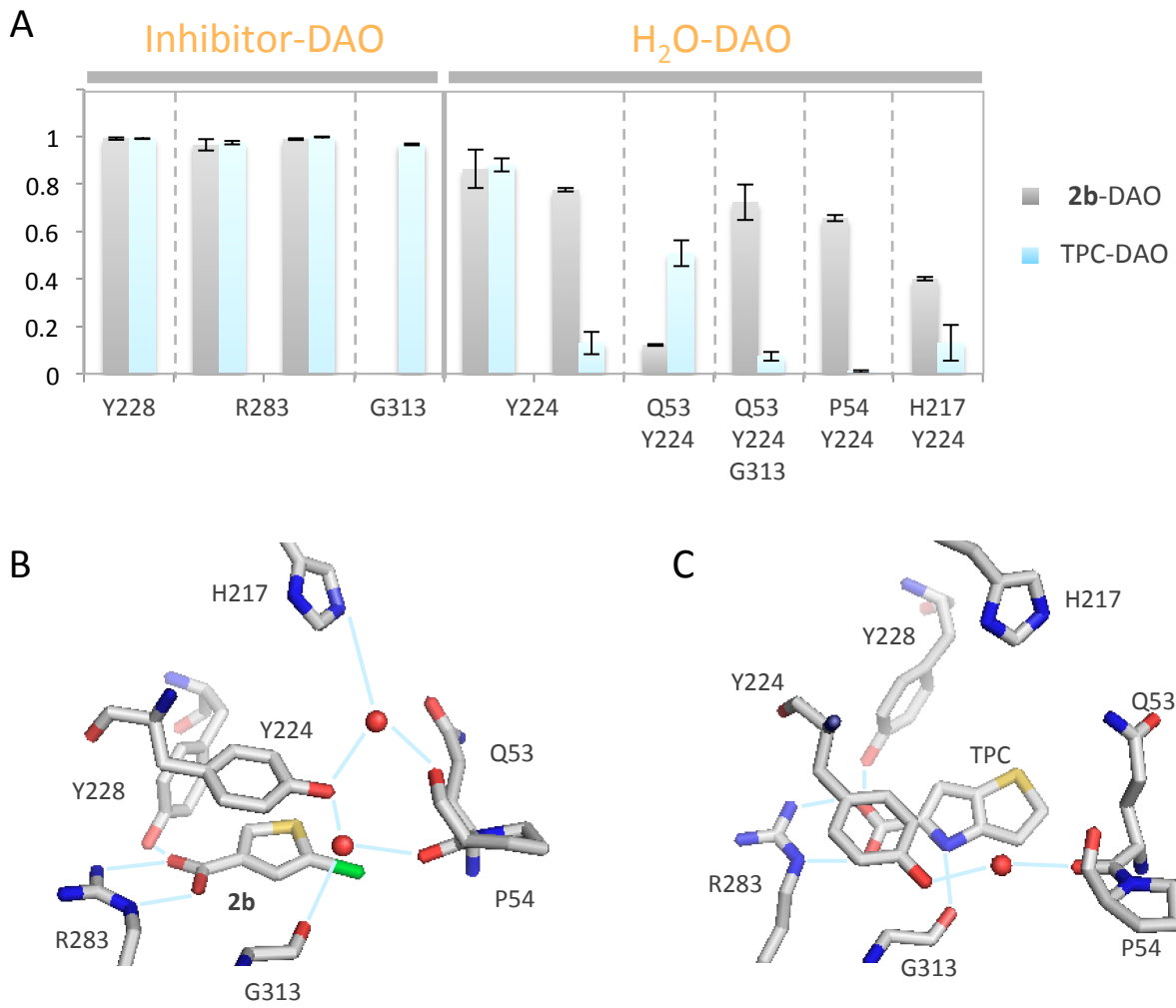
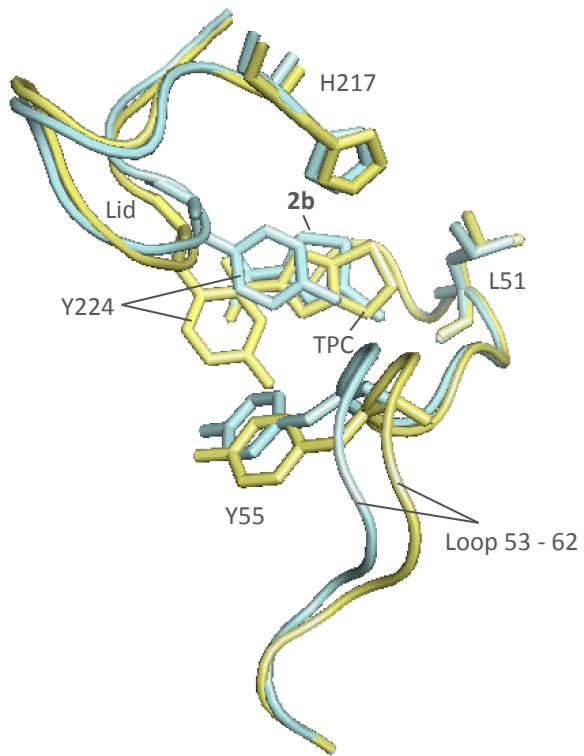
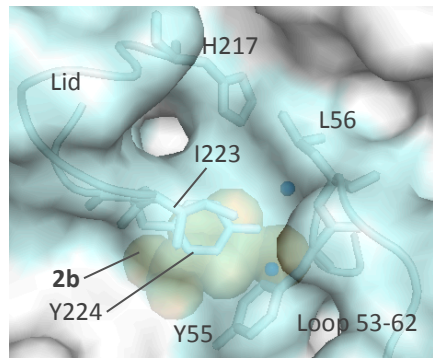


Fig. 4  
Kato et al. 2018

A



B



C

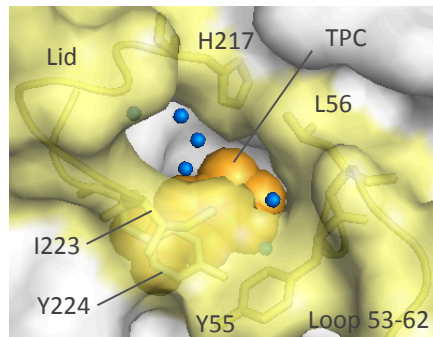
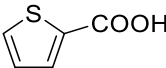
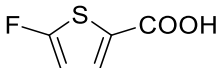
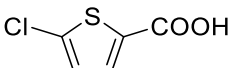
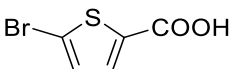
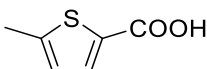
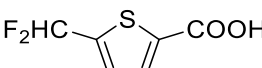
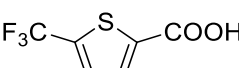
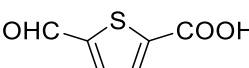
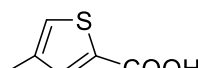
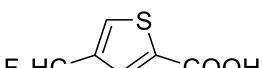
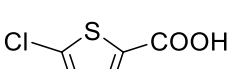
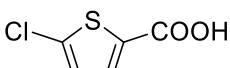


Fig. 5

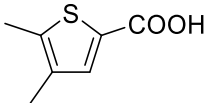
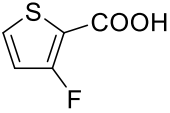
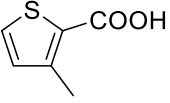
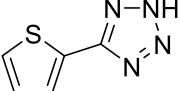
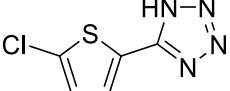
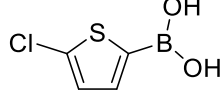
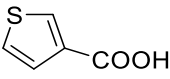
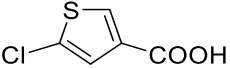
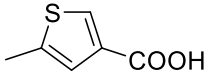
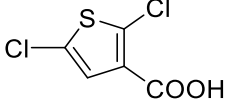
Kato et al. 2018

## Tables and Schemes

**Table 1 Inhibition of human DAO by low molecular weight thiophene carboxylic acids**

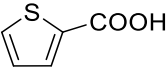
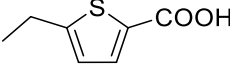
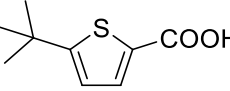
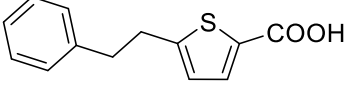
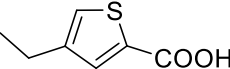
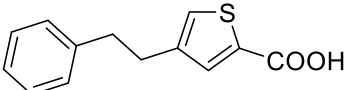
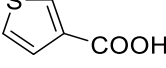
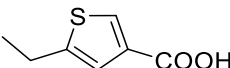
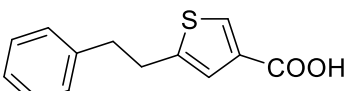
Cmpd	Structure	IC <sub>50</sub> (μM)
<b>1a</b>		7.8 ± 1.7
<b>1b</b>		1.4 ± 0.1
<b>1c</b>		0.72 ± 0.07
<b>1d</b>		1.3 ± 0.2
<b>1e</b>		4.6 ± 0.5
<b>1f</b>		8.8 ± 1.3
<b>1g</b>		21 ± 2
<b>1h</b>		>100
<b>1i</b>		1.3 ± 0.2
<b>1j</b>		1.3 ± 0.1
<b>1k</b>		0.090 ± 0.016
<b>1l</b>		0.36 ± 0.04



1m		$7.3 \pm 0.7$
1n		>100
1o		>100
1p		>100
1q		>100
1r		>100
2a		$4.4 \pm 0.6$
2b		$0.036 \pm 0.007$
2c		$0.22 \pm 0.02$
2d		$27 \pm 1$

---

**Table 2 Inhibition of human DAO by thiophene carboxylic acids containing a branched chain**

Cmpd	Structure	IC <sub>50</sub> (μM)
<b>1a</b>		7.8 ± 1.7
<b>1s</b>		>100
<b>1t</b>		>100
<b>1u</b>		>100
<b>1v</b>		>100
<b>1w</b>		55 ± 2
<b>2a</b>		4.4 ± 0.6
<b>2e</b>		38 ± 3
<b>2f</b>		39 ± 2

**Table 3 Calculated binding free energies and their components (kcal mol<sup>-1</sup>) for the 2b-DAO and TPC-DAO complexes**

	2b-DAO Chain A	2b-DAO Chain B	TPC-DAO chain A	TPC-DAO chain B
$\Delta E_{\text{vdw}}$	-21.4 ± 0.2	-20.5 ± 0.3	-21.4 ± 0.2	-21.6 ± 0.2
$\Delta E_{\text{elec}}$	52.9 ± 0.5	43.3 ± 0.6	39.9 ± 0.6	32.3 ± 0.5
$\Delta E^{\text{MM}}$	31.5 ± 0.5	22.8 ± 0.5	18.5 ± 0.6	10.6 ± 0.5
$T\Delta S^{\text{MM}}$	-26.1275	-26.4850	-26.6865	-27.2518
$\Delta G^{\text{MM}}$	57.6	49.3	45.2	37.9
$\Delta G^{\text{solv}}_{\text{polar}}$	-64.4 ± 0.5	-57.1 ± 0.5	-51.9 ± 0.6	-44.4 ± 0.5
$\Delta G^{\text{solv}}_{\text{nonpolar}}$	-2.840 ± 0.007	-2.781 ± 0.007	-2.788 ± 0.008	-2.757 ± 0.009
$\Delta G^{\text{solv}}$	-67.2 ± 0.5	-59.9 ± 0.5	-54.7 ± 0.6	-47.1 ± 0.5
$\Delta G_{\text{bind}}$	-9.6	-10.6	-9.5	-9.2
$\Delta G_{\text{exp}}^{\text{a}}$	-10.63		-11.68	
$\Delta G_{\text{Y224}}^{\text{b}}$	-1.57 ± 0.03	-1.44 ± 0.03	-0.69 ± 0.03	-0.73 ± 0.03
$\Delta G_{\text{G313}}^{\text{b}}$	-0.33 ± 0.03	-0.55 ± 0.02	-2.02 ± 0.05	-2.04 ± 0.05

<sup>a</sup> Calculated values from IC<sub>50</sub>.

<sup>b</sup> Results from the residue-based decomposition.

**Table 4 Residue-based energy decomposition on Tyr224 (kcal mol<sup>-1</sup>)**

	$\Delta G_{\text{vdw},\text{Y224}}^{\text{a}}$	$\Delta G_{\text{elec},\text{Y224}}^{\text{a}}$	$\Delta G_{\text{polar},\text{Y224}}^{\text{solv a}}$	$\Delta G_{\text{nonpolar},\text{Y224}}^{\text{solv a}}$	$\Delta G_{\text{Y224}}^{\text{a}}$
<b>2b-DAO</b> Chain A	-2.69 ± 0.02	1.00 ± 0.05	0.24 ± 0.05	-0.117 ± 0.001	-1.57 ± 0.03
<b>2b-DAO</b> Chain B	-2.68 ± 0.03	0.88 ± 0.05	0.47 ± 0.04	-0.114 ± 0.001	-1.44 ± 0.03
TPC-DAO Chain A	-1.93 ± 0.02	1.22 ± 0.05	0.16 ± 0.04	-0.133 ± 0.001	-0.69 ± 0.03
TPC-DAO Chain B	-1.90 ± 0.03	1.28 ± 0.04	0.02 ± 0.03	-0.133 ± 0.001	-0.73 ± 0.03

$$^{\text{a}}\Delta G_{\text{Y224}} = \Delta G_{\text{vdw},\text{Y224}} + \Delta G_{\text{elec},\text{Y224}} + \Delta G_{\text{polar},\text{Y224}}^{\text{solv}} + \Delta G_{\text{nonpolar},\text{Y224}}^{\text{solv}}$$

**Table 5 Distance between the residues that surround the active site in the S state.**

	1c-DAO <sup>a</sup>	2b-DAO <sup>a</sup>	2b-DAO <sup>b</sup>	Benzoate-DAO <sup>a</sup>
PDB ID/MD	5zja	5zj9	MD	2du8
Q53-H217	8.13 ± 0.06	8.28 ± 0.07	8.530 ± 0.009	8.38 ± 0.07
Q53-Y224	9.01 ± 0.03	9.16 ± 0.04	9.080 ± 0.007	9.15 ± 0.01
Q53-G313	4.96 ± 0.03	4.75 ± 0.06	4.685 ± 0.007	4.93 ± 0.05
H217-G313	10.25 ± 0.10	9.95 ± 0.03	10.193 ± 0.010	10.43 ± 0.08

<sup>a</sup> Average from all polypeptides in a unit cell

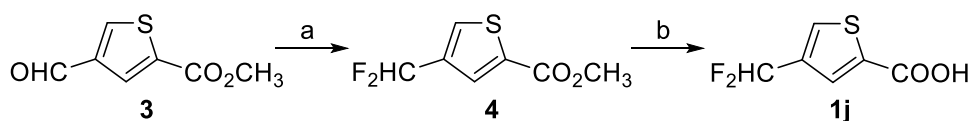
<sup>b</sup> Average throughout the trajectories.

**Table 6 Distance between the residues that surround the active site in the D state.**

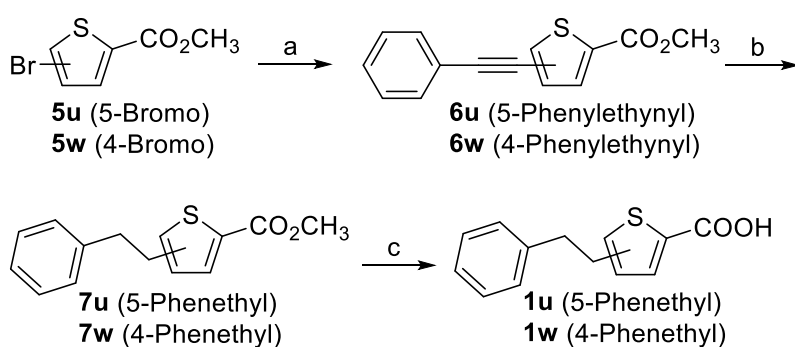
	TPC-DAO <sup>a</sup>	TPC-DAO <sup>b</sup>	CPC-DAO <sup>a</sup>	Imino DOPA-DAO <sup>a</sup>
PDB ID/MD	3znn	MD	3zno	2e82
Q53-H217	8.36 ± 0.09	8.588 ± 0.009	8.38 ± 0.12	8.61 ± 0.09
Q53-Y224	9.54 ± 0.04	9.667 ± 0.009	9.40 ± 0.24	9.77 ± 0.04
Q53-G313	5.06 ± 0.01	5.102 ± 0.011	5.50 ± 0.20	5.16 ± 0.10
H217-G313	10.52 ± 0.08	10.543 ± 0.010	11.02 ± 0.14	11.19 ± 0.13

<sup>a</sup> Average from all polypeptides in a unit cell

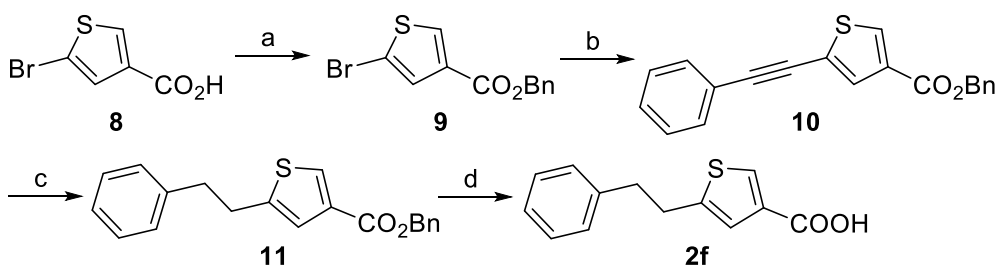
<sup>b</sup> Average throughout the trajectories.



**Scheme 1.** Synthesis of compound **1j**. Reagents and conditions: (a) Deoxo-Fluor, dichloromethane, rt; (b) NaOH, 1,4-dioxane-water, 100 °C.



**Scheme 2.** Synthesis of compounds **1u** and **1w**. Reagents and conditions: (a)  $\text{Ph}_3\text{P}$ ,  $\text{Pd}(\text{PhCN})_2\text{Cl}_2$ ,  $\text{CuI}$ , diisopropylamine, phenylacetylene, 70 °C; (b)  $\text{H}_2/\text{Pd-C}$ , EtOAc, 40-50 psi, rt; (c) NaOH, 1,4-dioxane-water, 100 °C.



**Scheme 3.** Synthesis of compound **2f**. Reagents and conditions: (a)  $\text{BnBr}$ ,  $\text{K}_2\text{CO}_3$ , acetonitrile, 80 °C; (b)  $\text{Ph}_3\text{P}$ ,  $\text{Pd}(\text{PhCN})_2\text{Cl}_2$ ,  $\text{CuI}$ , diisopropylamine, phenylacetylene, 70 °C; (c)  $\text{H}_2$ , Pd/C, EtOAc, 40 psi; (d) NaOH, 1,4-dioxane-water, 100 °C.